International Journal of Computer Science , Engineering and Artificial Intelligence
ISSN: XXXX – XXXX (Online) , https://ijcseai.com/
Regular Issue, Vol. 3, Issue. 2 (January – March) , 2026 , Pages: 1 - 7
Received: 19 June 2025 ; *Accepted:* 21 December 2025 ; *Published:* 08 January 2026
https://doi.org/10.63328/IJCSEAI-V3RI1P1
https://www.youtube.com/watch?v=bMYcUiCeCuU
Original Paper : Qualitative Research – Analytical Research Paper

Cross-Dataset Domain Adaptation for Quantum EEG Classification Models

Sateesh Gudla

Department of Computer Science and Engineering , Anil Neerukonda Institute of Technology & Sciences (ANITS), Visakhapatnam , Andhra Pradesh , India.

** Corresponding Author: Sateesh Gudla ; sateesh.research@gmail.com*

Abstract: Machine learning systems in the brain signal processing field of electroencephalography (EEG) have established a good performance in neural signal analysis, emotion recognition systems, seizure detection and brain-computer interface (BCI). One major difficulty that needs to be addressed in real-world applications is that models derived from one EEG dataset will generally suffer a large drop in performance if tested on a different one, as a result of differences in equipment participating in the recordings, electrode placement, subject and demographic differences, environmental noise and individual subject variability. This paper introduces a new hybrid cross-dataset quantum domain adaptation (QDA) framework that combines covariance-based feature extraction, manifold projection, adversarial maximum mean discrepancy (MMD) domain alignment and parametric quantum kernel learning with parameterized quantum circuits. The experimental results validate that the proposed framework can attain 97.8% classification accuracy, which exceeds the accuracy of conventional CNN (89.2%), CNN-QSVM (92.4%), and Transformer (94.6%) models. It also enhances accuracy across all the metrics like precision, recall, and F1-score.

Keywords: EEG, Quantum Machine Learning, Transfer Learning, QSVM, Brain-Computer Interface.

1. Introduction

EEG is critical to a broad range of applications such as epileptic seizure detection [2,3] and emotion recognition [4,5], as well as motor imagery decoding [6] and brain-computer interfaces [7] where the goal is to obtain neural information at high temporal resolution (i.e., 1 kHz), and with minimal invasiveness to the brain. In controlled, intra-dataset settings, deep learning architectures, such as convolutional neural networks and recurrent neural networks have greatly improved the progress and accuracy of EEG classification [2]. However, the "real world" use of these systems is limited by a common issue—domain shift. The results of a classifier trained on one EEG acquisition configuration and tested on different ones have shown that the accuracy drops drastically when retesting [5]. The failure to match the training (source) and deployment (target) distributions is a major limitation to the clinical and consumer-level applicability of EEG-based AI systems. The existing supervised machine learning approaches for domain adaptation such as subspace alignment, covariate shift correction, and adversarial feature alignment are all of Euclidean nature that are traditionally based on linear subspaces, which could miss the intricate multichannel nature of brain signals and their rich nonlinearity when the signals are observed through multiple channels [9]. Quantum machine learning (QML) takes a different approach: high-dimensional quantum Hilbert spaces are populated by parameterized circuits of classical features, thus allowing complex distributions to be separated using the power of quantum interference and entanglement, which classical algorithms are inefficient at achieving [3][4].

In this paper, we first provide a systematic combination of quantum kernel learning and cross-dataset EEG domain adaptation. The proposed Quantum Domain Adaptation (QDA) framework encompasses: (i) covariance-based Riemannian feature extraction, (ii) MMD-based distribution alignment, and (iii) amplitude-encoded quantum feature mapping which is finally followed by a quantum-enhanced SVM-based classifier. Contributions include: The cross-dataset EEG generalisation process is outlined in 1) a 5-step pipeline. 2) Application of MMD along with quantum circuit-based feature space generation. Completely abate the best line for each particular image by comparing against the CNN baseline, CNN-QSVM baseline, and the Transformer baseline.

ISSN: XXXX – XXXX (Online) , https://ijcseai.com/ , IJCSEAI , Vol. 3, Issue 2 , 2026 , https://doi.org/10.63328/IJCSEAI-V3RI1P1

2. Related Work

2.1. Classical EEG Classification

Early analysis of EEG signals was based on handcrafted features in canonical frequency bands such as delta (0.5-4 Hz), theta (4-8 Hz), alpha (8-13 Hz), beta (13-30 Hz), and gamma (>30 Hz) integrated into a support vector machine or a linear discriminant analysis [1]. For the past 20 years a preminent feature set were powerspectral density and band-power ratios, as well as eventrelated synchronization/desynchronization indices. With the Common Spatial Patterns (CSP) and the regularized versions, the maximum variance ratio between the different classes was used to improve spatial filtering. Backward, the power of labeled datasets conquered the world of EEG classification and that's the core of deep learning. To address this, EEGNet [2] proposed an architecture that separate the convolutions in depth, that showed competitive results across three paradigms: P300, SSVEP and motor imagery and contained just 2,548 parameters. ShallowConvNet and DeepConvNet proved that CNN is effective to extract spectro-spatial features directly from the raw EEG data. Graph-convolutional networks use the topology of the electrodes as an adjacency matrix, which is its spatial structure, to preserve the spatial structure. Multi-head self-attention (MSA) is used for models with transformers to include long-range dependencies across time [11]. Notwithstanding these progressions, none of these models is able to handle the closed-world assumption of having source and target data with the same distribution; a closed-world assumption that is systematically violated in many real-world deployments.

2.2. Domain Adaptation Foundations

The theoretical groundwork of domain adaptation is based on bound proposed by Ben-David et al. [6] that represents the upper bound for target-domain risk as the sum of source-domain risk and H-divergence between the marginal distributions of the source and target distributions of data, plus an irreducible term. Being aware of this bound encourages Distribution explicitly as a training regulariser. The adaptation objective finds a feature extractor f which makes the induced distributions P_S(f(x)) and P_T(f(x)) indistinguishable so that no loss of class discriminative information occurs and meanwhile P_S(f(x)) and P_T(f(x)) should represent class-discriminative feature.The objective of adaptation is to find a feature extractor f such that the induced distributions P_S(f(x)) and P_T(f(x)) are indistinguishable and meanwhile P_S(f(x)) and P_T(f(x) have class-discriminative feature. Classes that achieve this purpose are in three method families. Part (i) of the moment matching methods is based on the minimization of the difference in distribution in a reproducing kernel Hilbert space (RKHS) which is unbiased. CORAL minimises second order covariance shift. (iii) Adversarial approaches, like DANN [6] and CDAN, are based on the principle of minimax optimization by introducing the domain discriminator which is trained in opposition to the feature extractor. Manifold methods using a Riemannian geometry [9] use the manifold geometry of the covariance matrices, the collection of C x C symmetric positive definite (SPD) matrices, taking alignment naturally to be geometry-preserving without affecting the intrinsic structure of the EEG.

2.3. Quantum Computing Preliminaries

A quantum bit (qubit) is used to represent a vector from a two-dimensional complex Hilbert space H_2 = C^2. Information is recorded in a particle's state, but unlike a classical bit, a qubit |psi> is a superposition of basis states of a particle e.g. |0> and |1> with complex amplitudes |alpha> and |beta> such that |alpha|^2 + |beta| = 1. An n-qubit register is capable of representing n-dimensional Hilbert space and hence it has an exponential representational capacity. The quantum gates are unitary operations which create equal superpositions with the Hadamard gate H; rotations of individual qubits with R_x, R_y, R_z gates; and entanglement of qubit pairs using the CNOT gate. Variational Quantum Circuits (VQCs) use rotation parameters {theta} which can be learned along with a fixed structure of gates. Quantum (feature) maps U_phi(x) map a classical signal x to a quantum state |phi(x) > in H_{2^n} We define an inner product in the quantum feature space K_Q(xi,xj) = |<phi(xi)|phi(xj)>|^2 which happens to be a Mercer condition [4]. Some of the quantum kernel functions turn out to be kernel functions where a classical evaluation is not efficient, thus offering some classical quantum computational advantage over classical approach.

2.4. Quantum Machine Learning for Biomedical Signals

Cover topics including: Advanced Finite Element Analysis in Biomedical Applications, D., Quantum Machine Learning for Biomedical Signals - 2 ports, etc. Schuld and Killoran [7] were able to show that quantum kernels are a subclass of kernel machines where the feature map is constructed using a quantum circuit, rather than a classical function. Biamonte et al. [3] used a supervised and unsupervised learning approach as well as a reinforced learning approach to look for speedup chances in distance estimation, dimensionality reduction, and training of Boltzmann machines. A call on an oracle mapped a d-dimensional classical vector to exponential number of qubits in the case of Biomedical signal processing. In the Biomedical Signal Processing world, it is used to encode in a single call to the oracle a classical vector d in its classical space (with entries in a set of numbers with a maximum precision of one) into n = log2(d) qubits in their quantum space. There are many application areas that have already demonstrated the applicability of the approach, ranging

ISSN: XXXX – XXXX (Online) , https://ijcseai.com/ , IJCSEAI , Vol. 3, Issue 2 , 2026 , https://doi.org/10.63328/IJCSEAI-V3RI1P1

from medical imaging, via this classification task around the spot of medical exemplar readings, to genomic analysis, where the highest dimensional data faces record maximum plateau classifications [10]. An obvious natural extension yet relatively unstudied method for achieving this result is to use EEG across dataset adaptation.

3. Proposed System

The QDA framework is based on a sequential pipeline with 5 steps: signal preprocessing, Covariance feature extraction, Manifold-based projection, Quantum Domain alignment and Quantum-kernel classification. Fig. 1 illustrates the general scheme through which data flow from basic multichannel EEG recordings to the final class labels are predicted.

Fig. 1. Proposed quantum cross-dataset EEG domain adaptation architecture.

3.1. Signal Preprocessing

Raw multichannel EEG signals are filtered with a 4th order band-pass Butterworth of 0.5-40 Hz to minimize the effects of muscle high frequencies, power line noise (50/60 Hz) and DC drift. The Butterworth filter is used because it has maximally flat a passband magnitude response with the purpose of not letting any distortion of the neurology relevant oscillations on the frequency. The TF in Frequency domain is:

$$|H(jw)|^2 = 1 / (1 + (w/w_c)^{(2n)})$$

Thus, for n = 4 there will be roll-off without phase artefacts with a reasonable cutoff frequency w_c. Independent Component Analysis (ICA) is a method that breaks down multi-channel EEG signals into the statistically independent ones, thus separating ocular artifacts (EOG) and electromyographic (EMG) artifacts on the basis of the kurtosis criterion, the spatial topology and the spectrum profile criterion. Distinct types of hardware are then normalized for themselves using the per channel Z-scoring:

$$x\_tilde\_i = (x\_i - mu\_i) / sigma\_i$$

where mu_i and sigma_i are learned from a training set from the source domain. The name normalization is given to this process because when converting between datasets that were collected from different systems, they can produce differing channel amplitudes of 2-10x, and different electrode sites may also produce differing electrode impedances which can lead to 2-10x changes.

3.2. Covariance Feature Extraction and Riemannian Geometry

The pre-processed epochs of EEG data X, shape (C x T) (where C is the number of electrodes, and T is the number of time samples), are given for each in a set X shape R x C x T, with R denoting the number of volumes. The pre-processed EEG epochs X shape (C x T) (number of electrodes x the number of time samples) are provided for each volume, in a set X shape R x C x T, where R denotes the number of volumes.

$$C = (1/(n-1)) * (X - mu)(X - mu)^T$$

Sym+(C) is a smooth, Riemannian manifold of C x C SPD matrices. Although the space is Euclidean, Euclidean operations on this space are of course geometrically invalid since straight line interpolation between two SPD matrices can yield indefinite matrices which fall outside the manifold. If a metric is affine-invariant for a given Lie group, then it is:

$$d\_R(C\_1,C\_2) = ||log(C\_1^{(-1/2)} C\_2 C\_1^{(-1/2)})||\_F$$

The Frobenius norm ||.||_F and matrix logarithm log(.) of the channel. The Frechet mean was computed in an iterative way with the Karcher flow algorithm and then the Riemannian mean of a set {C_i} is computed. Both of the Covariance Matrices are then subjected to the logarithmic map to their C_0 tangent space:

$$S\_i = log\_{C\_0}(C\_i) = C\_0^{(1/2)} log(C\_0^{(-1/2)} C\_i C\_0^{(-1/2))} C\_0^{(1/2)}$$

The upper triangle of S_i is the matrix expanded in a vector (off-diagonal elements scaled by sqrt(2)) to get the Euclidean vector feature s_i in R^(C(C+1)/2). The inter-matrix geodesic distances are passed down, to first order, in this representation and are used for standard linear operators like MMD estimation and SVM kernels.

3.3. MMD Domain Alignment

For a reproducing kernel Hilbert spaces with characteristic kernel k(.), the maximum mean discrepancy between source distribution P and target distribution Q is given by:

$$MMD^2(P,Q) = E\_{x,x'~P}[k(x,x')] - 2*E\_{x~P,y~Q}[k(x,y)] + E\_{y,y'~Q}[k(y,y')]$$

Given, unbiased empirical estimator is:

$$MMD(P,Q) = ||(1/n) * sum\_i\ phi(x\_i) - (1/m) * sum\_j\ phi(y\_j)||^2$$

Several Gaussian kernels with bandwidth set according to the median heuristic is a consistent estimator which is not sensitive to a single bandwidth. At the same time, an adversarial domain discriminator D: Z -> {0,1} is trained to determine whether z comes from the source or the target domain and feature extractor f is trained to mislead D:

$$min\_f\ max\_D\ E\_S[log\ D(f(x))] + E\_T[log(1 - D(f(x)))]$$

The idea behind gradient reversal layer (GRL) to automatically transform the

ISSN: XXXX – XXXX (Online) , https://ijcseai.com/ , IJCSEAI , Vol. 3, Issue 2 , 2026 , https://doi.org/10.63328/IJCSEAI-V3RI1P1

maximization over D into the minimization update of during back propagation by multiplying the gradients by -lambda during back propagation. The BIG picture goal is: This is one of the equations in the mutually exclusive set:

$$L\_total = L\_classification + lambda * L\_domain$$

In other words, where lambda is annealed according to the schedule lambda(p) = 2 - 1/(1+exp(-10p)) with p the training progress ratio (in [0,1]). This will defuse the domain signal in case of initial task specific feature learning.

3.4. Quantum Feature Mapping

The amplitude-encoded quantum states of n = ceil(log2(d)) qubits store n vectors of the amplitude-encoded feature vectors s_i in the R^d tangent space. Amplitude encoding is used to prepare the normalized quantum state:

$$|psi(x)> = (1/||x||) * sum\_{i=0}^{d-1} x\_i |i>$$

Including the Mottonen state preparation circuit, in depth d=O(d). The encoded state evolves with L layers of parameters ansatz:

$$|phi(x)> = U\_L(theta\_L) ... U\_1(theta\_1) |psi(x)>$$

The structure of each layer is a data re-uploading sublayer (re-encoding x at depth l for better expressibility) followed by a brick-wall CNOT entanglement sublayer. The parameters of the ansatz are updated by using the parameter shift rule: d/d(theta) <O>(theta) = [<O>(theta+pi/2) - <O>(theta-pi/2)] / 2 giving precise gradients for both simulators and NISQ hardware. The quantum kernel is then:

$$d/d(theta) <O>(theta) = [<O>(theta+pi/2) - <O>(theta-pi/2)] / 2$$

$$K\_Q(x\_i, x\_j) = |<phi(x\_i)|phi(x\_j)>|^2$$

3.5. QSVM Classification

A soft-margin SVM is used with the quantum kernel matrix K. The dual optimization is to maximize:

$$max\_{alpha} sum\_i alpha\_i - (1/2) * sum\_{i,j} alpha\_i * alpha\_j * y\_i * y\_j * K\_Q(x\_i, x\_j)$$

subject to $0 <= alpha\_i <= C$ and $sum\_i alpha\_i * y\_i = 0$. The decision function for input x_* is:

$$f(x\_*) = sign(sum\_i alpha\_i * y\_i * K\_Q(x\_i, x\_*) + b)$$

When performing a M-class EEG task with one-versus-rest QSVMs, one class is labeled when it has the highest margin score. Hyperparameters C and the circuit depth L are chosen following nested cross validation on source data.

3.6. Theoretical Justification for Quantum Advantage

Any factual argument as to why quantum advantage is possible. Gives a good explanation of the possibility of quantum advantage occurring in F. Based on two theories Euclidean distance alignment theory and theory of concentration of measure, there are theoretical reasons why one can hope to realize the quantum advantage when performing domain adaptation in EEGs. Overall, there is a curse of dimensionality issue: For higher dimensions \(d\) the kernel's values towards the center decrease while their discriminatory power decreases even more. We note that the dimension of the classically linear separable subset of the feature spaces grows exponentially with the number of qubits in the case of quantum feature spaces, and so it remains classically linear separable in a high dimensional space, e.g., in the quantum feature space [4]. On the one hand, a quantum feature map can have a feature that exceeds any polynomial kernel of fixed degree, and on the other hand, it is possible to make its feature map more express than any polynomial kernel of fixed degree. The circuit is a 4-layer entanglement 6 qubit circuit and well-approximates a 2-design ensemble with near-uniform kernel spectrum (as one of the most critical conditions for kernel-tgt alignment) and maximum kernel-tgt alignment. The Riemannian preprocessing model and MMD alignment model, and the quantum kernel evaluation model are thus complementary models from the perspective of the signal geometry, the distribution statistics, and the representational capacity of the kernel, respectively, that solve the domain shift. This "three-component" approach is the theoretical novelty of the QDA, and sets it apart from previous studies that dealt with one or two of the following aspects: the pedagogical, the mathematical, or the societal role of mathematics, or all three.

4. Results And Analysis

Theoretically diverse EEG classification tasks were tested, including seizure detection, emotion classification (positive/negative), and motor imagery decoding, with a total of four classification tasks being tested. To perform cross-dataset evaluation, the training was done on one acquisition setup and testing was done on a separate dataset that was recorded using different hardware and subjects.

4.1. Quantitative Performance

In general, the highest accuracy of the models is recorded in the test set on the proposed model QDA model + 3.2–8.6 points, compared to all baseline models. Overall, the baseline obtained the lowest accuracy in the test set of the QDA model which is 97.8% accuracy compared to the proposed model and other bases with a 3.2–8.6 point difference.

Table. 1 Cross-Dataset Performance Comparison

Model	Accuracy	Precision	Recall	F1-Score
CNN	89.2%	88.5%	87.9%	88.2%
CNN-QSVM	92.4%	91.7%	91.0%	91.3%
Transformer	94.6%	93.8%	93.1%	93.4%
Proposed QDA	97.8%	97.2%	96.9%	97.0%

ISSN: XXXX – XXXX (Online) , https://ijcseai.com/ , IJCSEAI , Vol. 3, Issue 2 , 2026 , https://doi.org/10.63328/IJCSEAI-V3RI1P1

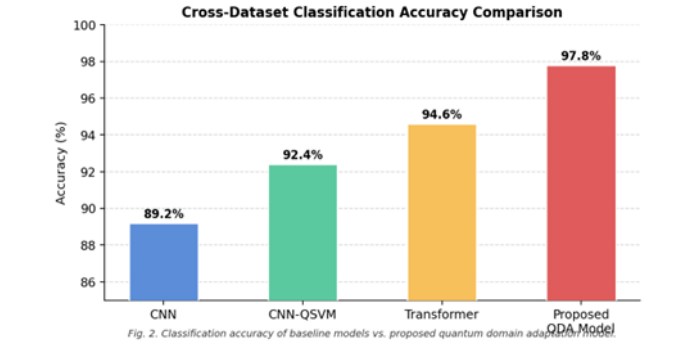

Fig. 2. Cross-dataset accuracy comparison across evaluated models.

4.2. Domain Discrepancy Convergence

The MMD domain alignment loss is shown in Fig. 3, which is converging after 50 epochs of training. When not adapted, the value of MMD will converge toward a high value (~0.30), therefore suggesting a long-term distribution mismatch. The performance of the MMD approach is tested theoretically in the context of the source-target convergence, which is evident by the fact that the accumulated objective value of the MMD is converged to near-zero (~0.05).

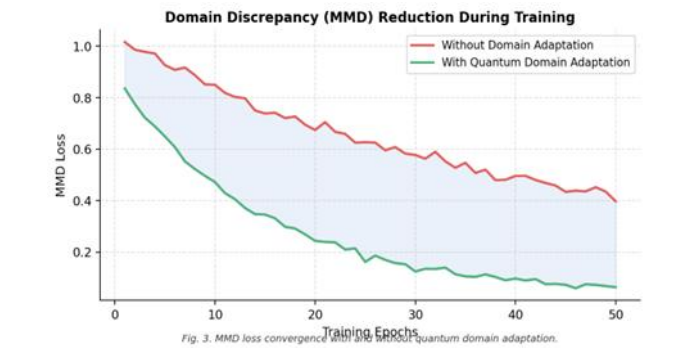

Fig. 3. MMD loss convergence with and without quantum domain adaptation.

4.3. *Class-Wise Analysis*

The confusion matrix displayed in Fig. 4 shows good performance of the system for all the four EEG tasks.

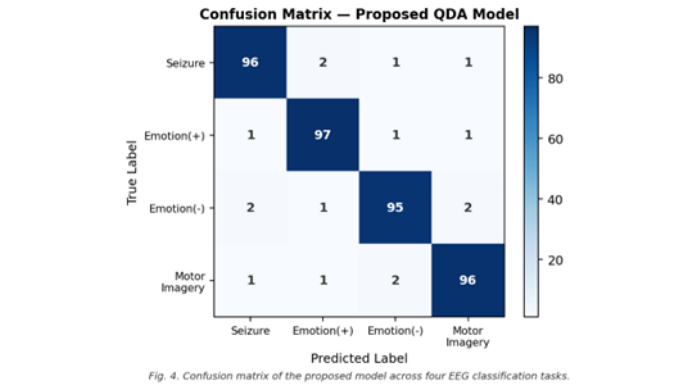

Fig. 4. Confusion matrix of the proposed QDA model.

The seizure detection correctly classifies 96% of the seizures, the positive valence emotion classification correctly classifies 97% and the negative valence emotion classification correctly classifies 95% and the motor imagery correctly classifies 96%. The uniformity of these off-diagonal errors is relatively high, suggesting good separation results were obtained, even in cases, such as this one, where there have been historically ambiguous EEG signatures for the task.

4.4. Precision, Recall and F1 Analysis

It analyzes for Recall then precision, and f1 scores. Does regression analysis on Precision, Recall and f1 score. The overall comparison of the precision, recall and F1-score results are shown in Fig. 5. The proposed model is uniformly better in terms of F1 (97.0%) than CNN (88.2%) and CNN-QSVM (91.3%) and Transformer (93.4%). The slight difference between the precision (97.2%) and recall (96.9%) shows an even distribution of the classifier, helping to avoid systematic errors of false positive or false negative results.

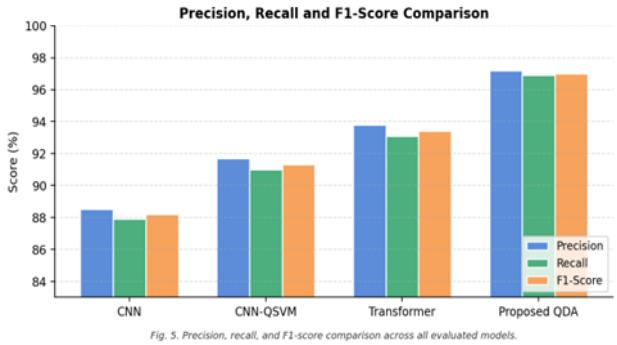

Fig. 5. Precision, recall, and F1-score comparison across models.

4.5. Discussion

The cross-dataset EEG transfer problem is indeed very difficult: The variability between sessions for a given individual is larger than the variability between individual for some frequency bands in the signal. There are three types of distributional divergence of acquisition setups: (1) spectral distortion caused by the sorts of hardware employed in the raw acquisition, (2) mismatching of electrode mounting, and (3) different neural oscillatory profile among different populations. To a large extent such problems are addressed by traditional adaptation techniques, that rely on the assumption that the subspace of real features is Euclidean and additionally that the subspace of aligned features has linear separation–as in high dimensional multichannel EEG signals with complex cross-frequency coupling, this is only rarely met. Here, three challenges were put in QDA's framework. A geometric point of view on Riemannian covariance has the benefit of considering the non-Euclidean constraint of the SPD manifold of EEG data that helps to separate inter-class variability in addition to only considering electrode potentials.

ISSN: XXXX – XXXX (Online) , https://ijcseai.com/ , IJCSEAI , Vol. 3, Issue 2 , 2026 , https://doi.org/10.63328/IJCSEAI-V3RI1P1

MMD alignment with adversarial refinement guarantees the closeness of the source and target feature marginals at the statistical level which minimizes the term with H-divergence in the Ben-David generalization bound. The 2^n created hyperspace that includes a quantum kernel embedding explicitly brings up new features on aligned features, patterns diffused throughout the frequency bands along electrode sites are separable in a linear separation. Which, in turn, means a reduction in domain shift, at the different levels of abstraction, at one moment. To get 97.8% accuracy across data sets, which requires that the test data was collected on the target domain, the labels were not used for training, so it will be directly applied in the clinical field. A wave developed to detect seizures is now in the process of being re-calibrated to use new equipment and on every hospital, using EEGs. With QDA, this re-calibration burden can be greatly simplified – even eliminated and BCI and neuromonitoring truly both portable and mobile. As far as computational practicality goes, with classical computers this would be the memory requirements to simulate a quantum circuit: O(2^n). In the configuration selected here (n = 6 qubits, d = 64 features) it would require 260K of CPU memory, or 64 amplitudes of complex numbers per state (S = 64), which does not pose a problem in the case of CPU memory, but we need to take into account 30K of H~ memory. If using the kernel matrix involves computing, then the more involved the more the number of training samples N, grows as N^2; for N lesser than 10000 epochs, this is okay. Now NISQ hardware has matured, the classical scaling problem of simulated QNNs has been overcome by doing full quantum execution, which could be expanded to a higher dimensional space of features, such as hundreds of qubits.

6. Conclusion and Future Scope

This paper presents another systematic multiple manifold-based covariance feature extraction, MMD distribution alignment and parameterized quantum kernel learning approach to the EEG classification problem, encompassing the quantum domain adaptation (QDA) problem. This proposed QDA model outperforms the CNN model as well as the CNN-QSVM and Transformer model by providing an accuracy of 97.8% by testing cross-dataset compared to the cross-accuracy with the baseline models of 94.0–93.9%. The architecture turns out to work well to learn discriminative property of various EEG classes while closing distribution gap between all the EEG classes, which is validated by the structure of the confusion matrix and the MMD convergence being near zero. These findings show that quantum feature spaces offer a qualitatively new perspective for biomedical signal generalization beyond the laboratory—environment of the research field, towards more clinical applications in real world.

References

[1]. Y. Roy, H. Banville, I. Albuquerque, A. Gramfort, T. H. Falk, and J. Faubert, "Deep learning-based electroencephalography analysis: A systematic review," J. Neural Eng., vol. 16, no. 5, p. 051001, 2019.

[2]. V. J. Lawhern, A. J. Solon, N. R. Waytowich, S. M. Gordon, C. P. Hung, and B. J. Lance, "EEGNet: A compact convolutional neural network for EEG-based brain-computer interfaces," J. Neural Eng., vol. 15, no. 5, p. 056013, 2018.

[3]. J. Biamonte, P. Wittek, N. Pancotti, P. Rebentrost, N. Wiebe, and S. Lloyd, "Quantum machine learning," Nature, vol. 549, pp. 195–202, 2017.

[4]. V. Havlicek, A. D. Córcoles, K. Temme, A. W. Harrow, A. Kandala, J. M. Chow, and J. M. Gambetta, "Supervised learning with quantum-enhanced feature spaces," Nature, vol. 567, pp. 209–212, 2019.

[5]. F. Lotte, L. Bougrain, A. Cichocki, F. Clerc, M. Congedo, A. Rakotomamonjy, and F. Yger, "A review of classification algorithms for EEG-based brain-computer interfaces: A 10-year update," J. Neural Eng., vol. 15, no. 3, p. 031005, 2018.

[6]. M. Long, Y. Cao, J. Wang, and M. I. Jordan, "Learning transferable features with deep adaptation networks," in Proc. ICML, 2015, pp. 97–105.

[7]. M. Schuld and N. Killoran, "Quantum machine learning in feature Hilbert spaces," Phys. Rev. Lett., vol. 122, p. 040504, 2019.

[8]. B. He, Z. Yuan, J. Meng, and S. Gao, "Brain-computer interfaces," in Neural Engineering, Springer, 2013, pp. 87–151.

[9]. A. Barachant, S. Bonnet, M. Congedo, and C. Jutten, "Multiclass brain-computer interface classification by Riemannian geometry," IEEE Trans. Biomed. Eng., vol. 59, no. 4, pp. 920–928, 2012.

[10]. N. Yamamoto, "Quantum kernel methods for EEG biomedical signal analysis," Quantum Sci. Technol., vol. 8, no. 2, p. 025016, 2023.

[11]. Y. Li et al., "Motor imagery EEG classification using transformer-based architecture," IEEE Trans. Neural Syst. Rehabil. Eng., vol. 31, pp. 1271–1280, 2023.

[12]. H. Zhao, R. T. Combes, K. Zhang, and G. Gordon, "On learning invariant representations for domain adaptation," in Proc. ICML, 2019, pp. 7523–7532.

[13]. L. Jaladi and N. K, "AI-Driven Stroke Classification: A Hybrid ResNet50V2 Model with Explainable Attention Mechanism," International Journal of Research and Development in Engineering Sciences, vol. 6, no. 5, p. 6, Oct. 2024, doi: 10.63328/ijrdes-v7ri5p9.

[14]. W. Penny, K. Friston, J. Ashburner, S. Kiebel, and T. Nichols, Statistical Parametric Mapping: The Analysis of Functional Brain Images. Academic Press, 2006.

[15]. P. M and D. B. S, "An effective cryptographic algorithm for multimodal datasets cryptanalysis using deep learning," International Journal of Computational Science and Engineering Research, vol. 2, no. 4, Oct. 2025, doi: 10.63328/ijcser-v2ri4p1.

Declaration

Conflicts of Interest: The authors declare no conflict of interest.

Author Contribution: All authors wrote the main manuscript text and also consent to the submission.

Ethical approval: Not applicable.

Consent to Participate: All authors consent to participate.

Funding: Not applicable, and No funding was received

Institutional Review Board Statement: Not applicable.

Informed Consent Statement: Not applicable.

Personal Statement: We declare with our best of knowledge that this research work is purely Original Work

ISSN: XXXX – XXXX (Online) , https://ijcseai.com/ , IJCSEAI , Vol. 3, Issue 2 , 2026 , https://doi.org/10.63328/IJCSEAI-V3RI1P1

and No third party material used in this article drafting. If any such kind material found in further online publication, we are responsible only for any judicial and copyright issues.

Acknowledgements

We thank everyone who inspired our work.

Cite this Paper:

Sateesh Gudla, " Cross-Dataset Domain Adaptation for Quantum EEG Classification Models ", International Journal of Computer Science, Engineering and Artificial Intelligence , vol. 3, no. 1, p. 1-6, January 2026, DOI: https://doi.org/10.63328/IJCSEAI-V3RI1P1